
This is an electronic reprint of the original article.
This reprint may differ from the original in pagination and typographic detail.

Khodaparast, Aryorad ; Hassani, Mohammadjavad; Azimi, Erfan ; Adabi, M. Ebrahim; Adabi, Jafar; Pouresmaeil, Edris

Circuit Configuration and Modulation of a Seven-Level Switched-Capacitor Inverter

Published in:
IEEE Transactions on Power Electronics

DOI:
[10.1109/TPEL.2020.3036351](https://doi.org/10.1109/TPEL.2020.3036351)

Published: 06/11/2020

Document Version
Peer-reviewed accepted author manuscript, also known as Final accepted manuscript or Post-print

Please cite the original version:
Khodaparast, A., Hassani, M., Azimi, E., Adabi, M. E., Adabi, J., & Pouresmaeil, E. (2020). Circuit Configuration and Modulation of a Seven-Level Switched-Capacitor Inverter. *IEEE Transactions on Power Electronics*, 36(6), 7087-7096. Article 9250604. <https://doi.org/10.1109/TPEL.2020.3036351>

© 2020 IEEE. This is the author's version of an article that has been published by IEEE. Personal use of this material is permitted. Permission from IEEE must be obtained for all other uses, in any current or future media, including reprinting/republishing this material for advertising or promotional purposes, creating new collective works, for resale or redistribution to servers or lists, or reuse of any copyrighted component of this work in other works.

Circuit Configuration and Modulation of a seven-level Switched-Capacitor Inverter

Aryorad Khodaparast, Mohammadjavad Hassani, Erfan Azimi, M. Ebrahim Adabi, Jafar Adabi, and Edris Pouresmaeil, *Senior Member, IEEE*

Abstract—In this paper, a step-up seven-level inverter supplied by a single DC source suitable for renewable energy application is presented. Forming the desired output is realized by charging capacitors and synthesizing them based on switched-capacitor concept. This structure is praised for the ability of sensor-less voltage balancing of the capacitors, reducing control complexity to produce a bipolar staircase waveform. It also benefits from regenerative performance, avoiding unwanted capacitors overvoltage. Phase Disposition Pulse Width Modulation (PD-PWM) technique is utilized to control the circuit operation. Furthermore, a comparison with other recent topologies reveals that losses, number of semiconductor devices, and gate driver circuits are reduced. Theoretical analysis is verified through a laboratory prototype implementation. Experimental results under various types of loads approve the performance of the proposed inverter and validity of the design. Finally, maximum experimental efficiency of 94.3% (115 V, 250 W load) was reached.

Index Terms—multilevel inverter; single-source; switched-capacitor; step-up converter; self-balancing.

I. INTRODUCTION

Nowadays, increasing use of Renewable Energy Sources (RESs) due to the end of fossil energy and the necessity of reducing gas emissions have been influencing energy arena. Mostly these sources generate DC power while the conventional power systems are in AC form. Hence, for connecting these energy sources to the power grid, various types of DC-AC converters are introduced. Among all, Multi-Level Inverters (MLIs) have significantly drawn the attention of electrical engineers. These structures are praised for their better quality of output waveform, lower voltage stresses (dv/dt), less THD (Total Harmonic Distortion) and their ability to operate in lower switching frequencies [1]. MLIs have become popular and have some advantages in many applications such as fuel cells [2], solar panels [3], electric vehicles [4], motor drives [5], wind turbines and grid-connected applications [6-7]. The most applicable structures among them include Cascaded H Bridges (CHB) [8], Neutral Point Clamped

(NPC) [9], Flying Capacitor (FC) [10] and Switched Capacitor (SC) [11].

The CHB topology is famous for its modularity and simplicity to expand, leading to an increase in the number of output voltage levels. According to the aforementioned pros, by increasing H-bridge cells, the number of required switches and independent DC voltage sources are raised in CHB structures [12]. In this circumstance, implementation complexity, cost increment and bulky system caused by low-frequency operation of the CHB structures increase [13]. To alleviate these problems, applying asymmetrical DC voltage sources [14] and a cascaded transformer [15] are proposed. Both NPC and FC structures suffer from voltage balancing complexity of DC-Link capacitors. Moreover, high number of semiconductor components decrease the reliability of the circuit and its application. Also, among their active switches they don't have the ability of equal voltage sharing, both statically and dynamically [16-17].

Switched-Capacitor Multi-Level Inverters (SCMLIs) are therefore introduced in order to cover the abovementioned problems. Many new converters were designed to decrease the number of components such as semiconductors, DC sources, and capacitors to lessen costs but they have other drawbacks in their structure [18-19].

One of the most essential traits for such converters (especially in many renewable energy applications with low voltage DC source such as solar systems) which standard MLI circuits do not possess is boosting capability. The voltage boosting is realized by charging capacitors and then summing the capacitors voltages up in a series connection to be applied to the output, eliminating the need for bulky transformers or inductors [20-21].

Another crucial character for an SCMLI circuit is whether the inverter can be used in application with regenerative load feature or not. For any inverter circuits, every time interval that the polarity of the output voltage and current are the same, the power is supplied to the load and the inverter is in “inverting” mode. Otherwise, the inverter is in “rectification or regeneration” mode [22]. Application with regenerative loads

Manuscript received March 28, 2020; revised August 24, 2020; accepted October 22, 2020.

A. Khodaparast, M.J. Hassani, E. Azimi, and J. Adabi are with the Faculty of Electrical and Computer Engineering, Babol Noshirvani University of Technology, Babol 47148-71167, Iran (e-mail: a.khodaparast.q@gmail.com; javadhasani@gmail.com; Erfan.azimi.eab@gmail.com; j.adabi@nit.ac.ir).

M. E. Adabi is a Postdoctoral Researcher with Ecole Centrale de Nantes in Laboratoire des Sciences du Numériques de Nantes, Nantes, France, (e-mail: ebrahim.adabi@ec-nantes.fr).

E. Pouresmaeil is with the department of electrical engineering and automation (EEA) at Aalto University, Espoo, Finland. (e-mail: edris.pouresmaeil@aalto.fi).

require inverters with a bidirectional power flow preventing the capacitors from over-charging and potential damages. Ergo, the excess charge is fed to the input source. In this case, [23-26] introduced new SCMLI structures with regenerative load feature. Also, they all have the boosting capability except for [26] where the maximum amplitude of the output is equal to the input source. Besides, the capacitors' voltages in [23-25] are self-balanced and there is no need for any extra balancing control system. However, the number of components required for these topologies are high. The structures introduced in [20], [27-29] can boost the input voltage, but as they use series diodes in their capacitors' charging paths, they lack the regenerative load feature.

This paper presents a seven-level single source step-up boost inverter with a low number of components. It requires two capacitors to boost the input voltage up to $3V_{in}$. Phase Disposition Pulse Width Modulation (PD-PWM) control strategy is used to produce the desired output waveform with lower harmonic content. By charging or discharging capacitors in small sequential time intervals, they would face the least possible voltage drop. This structure is suitable for a vast range of low voltage single-source application using photovoltaic, batteries, and fuel cells (without any need for bulky and sometimes low efficient inductors).

This study is organized as follows: The working principles of the proposed circuit are brought in Section II, containing capacitors charging pattern, different operation modes and a brief note on circuit modulation method. Section III reveals the determination of circuit capacitors, power loss calculation and a comparative discussion of the presented structure against several recent topologies. Further, design considerations and results of a test setup including both regenerative and non-regenerative load behaviors are added in Section IV. Conclusions are finally represented in Section V.

II. PRINCIPLE OF OPERATION

Fig. 1 describes the overall structure of the proposed seven-level boost inverter and its operating modes. It consists of a single DC source (V_{dc}) which charges the capacitors C_1 and C_2 one after the other, directly. Also, the inverter supplies the load by a few numbers of switches (maximum number of four) per each level which will increase the overall efficiency of the converter. However, this converter produces 7-levels of voltage ($\pm 3V_{dc}$, $\pm 2V_{dc}$, $\pm 1V_{dc}$, and 0) with only 2 capacitors, 9 switches, and 9 driver circuits.

A. Capacitor charging

The capacitors C_1 and C_2 can be charged up to V_{dc} by the input source at different operation modes when they are not being used to generate the output. Thus, the capacitors' voltages would be kept in an acceptable range and well balanced. This means that there is no need for any voltage feedback from the capacitors to the control system.

It is worth noting that the proposed converter has power regeneration capability which means that the capacitors can be automatically discharged to the source if overcharged (as an example is brought in Fig. 1). Therefore, the converter can be

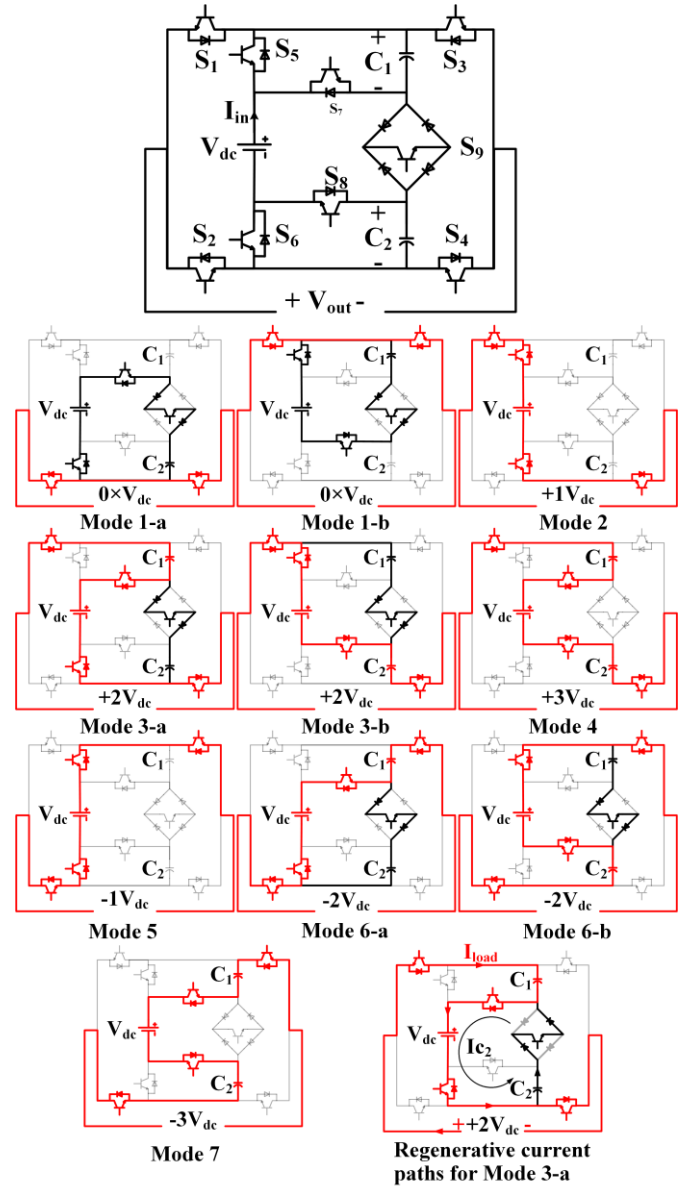


Fig. 1. The Overall structure of the proposed seven-level boost inverter and its operating modes

also used for motor drive purposes. Note that for non-regenerative loads, the structure can operate normally and S9 could be simplified as a unidirectional switch.

B. Operation modes

Fig. 1 also shows the different operation modes of the proposed converter and its switching states to generate the output voltage levels. Furthermore, the capacitor charging paths are added. These modes are described below:

1) Mode 1-a, 1-b: $0V_{dc}$

This mode of operation which produces zero voltage at the output can be applied by two different switching states; by using either switches S_2 & S_4 or S_1 & S_3 . In each of these states, one of the capacitors can be charged. By applying these states sequentially, both of the capacitors voltages will stay balanced.

2) Mode 2: $+1V_{dc}$

In this mode input voltage is directly applied to the load through switches S_1 , S_5 , S_6 , and S_4 .

3) Mode 3-a, 3-b: +2V_{dc}

This mode can be applied by two different switching states. In the first state, a series connection of the supply voltage and C₁ generates the output while C₂ is being charged (mode 3-a). In the second state, C₁ is replaced by C₂ (mode 3-b). Similar to mode 1, both states are applied sequentially to maintain the capacitors voltage balance.

4) Mode 4: +3V_{dc}

To generate +3V_{dc} across the load both of the capacitors and the input source are used meaning that at this stage no capacitor can be charged.

5) Mode 5-7: -1V_{dc}, -2V_{dc}, -3V_{dc}

These voltages can be generated in the same way as their positive counterparts. The only difference is that switches S₂ & S₃ must be turned on instead of S₁ & S₄.

C. PD-PWM modulation method

Phase Disposition Pulse Width Modulation (PD-PWM) technique has been adapted to control the sensor-less operation of the proposed converter in offline mode. As shown in Fig. 2, six level-shifted PWM carriers (with an amplitude of A and frequency of f_{pw}) are compared to a sine reference signal (V_{ref} = A_{ref} sin(2πf_{ref}t)) in the DSP controller. As a result, the appropriate gate signals for the circuit switches are produced in predetermined time intervals. The main benefit of this method is its simplicity in realization, fast response and a waveform with lower harmonic content [24].

The rules of operation under such technique are revealed in Table I. Where V_{tri1,2,...,6} are six carrier (PWM) signals (with shifted levels and identical amplitudes) generated to be compared with the reference signal. Also, the output waveform and capacitors voltages for different modes of operations are illustrated over one period in Fig. 2.

III. DESIGN CONSIDERATIONS

A. Capacitor Calculations

It is essential to make sure that the voltages of the two capacitors do not drop below a permissible value, as they have the task of generating the output voltage with magnitudes higher than 1V_{dc}. For this, the amount of energy they store and pump to the output should be measured to calculate the capacitances. The capacitors voltages and their charging and discharging patterns at different modes of operation are shown in Fig. 2. Maximum discharge happens for a resistive load as the maximum current is drawn in mode 4 in which both capacitors are supplying the output.

The capacitors' voltage drop occurs in [t_a, t_b]. To calculate the required capacitances, the discharge of the capacitors in this time interval must be measured for a permissible voltages drop at the desired output load. The Charge and discharge cycle of the capacitors in [t_a, t_b] is assumed to happen for n times and m = (0, 1, 2, ..., n). As can be seen in Fig. 2, discharging cycles of C₁ starts at t_{2m}^{C1} and ends at t_{2m+1}^{C1}. Similarly, the discharge of C₂ happens between [t_{2m}^{C2}, t_{2m+1}^{C2}] cycles. The amount of electrical charge (Q) discharged from t_{2m} to t_{2m+1} of the capacitors C₁ and C₂ are [23]:

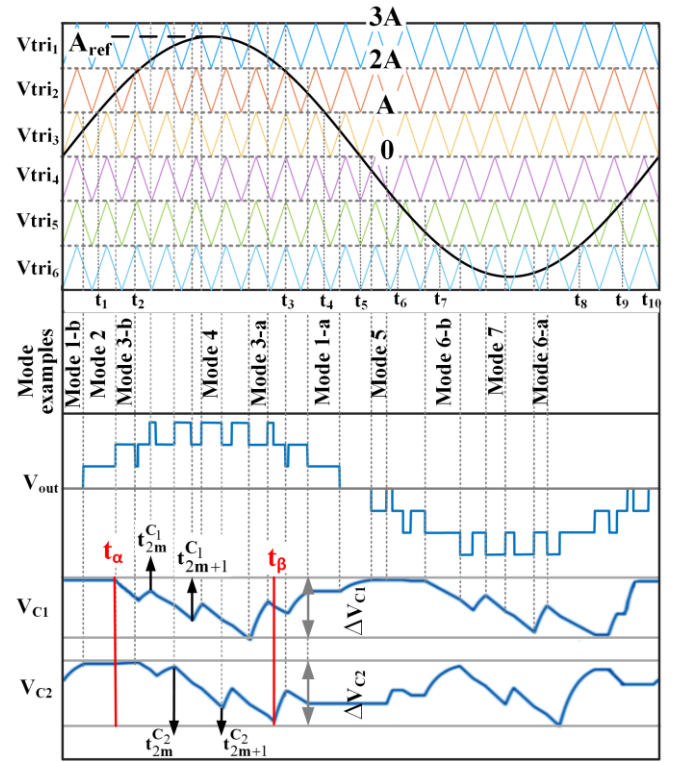


Fig. 2. PD-PWM modulation strategy

TABLE I
PD PWM SWITCHING MODES AND RELEVANT STATES OF CHARGE

Amplitude of V _{ref}	mode	Output voltage	C ₁	C ₂
V _{ref} > V _{tri1}	Mode 4	+3V _{dc}	▲	▼
V _{tri2} < V _{ref} < V _{tri1}	Mode 3-a	+2 V _{dc}	▲	▼
V _{tri2} < V _{ref} < V _{tri1}	Mode 3-b	+2 V _{dc}	▼	▲
V _{tri3} < V _{ref} < V _{tri2}	Mode 2	+1 V _{dc}	-	-
V _{tri4} < V _{ref} < V _{tri3}	Mode 1-a	0	▲	-
V _{tri4} < V _{ref} < V _{tri3}	Mode 1-b	0	-	▲
V _{tri5} < V _{ref} < V _{tri4}	Mode 5	-1 V _{dc}	-	-
V _{tri6} < V _{ref} < V _{tri5}	Mode 6-a	-2 V _{dc}	▲	▼
V _{tri6} < V _{ref} < V _{tri5}	Mode 6-b	-2 V _{dc}	▼	▲
V _{ref} < V _{tri6}	Mode 7	-3 V _{dc}	▼	▼

$$\Delta Q_m^{C1} = \int_{t_{2m}^{C1}}^{t_{2m+1}^{C1}} I_{out} \cdot \sin(\omega t) \cdot dt \quad (1)$$

$$\Delta Q_m^{C2} = \int_{t_{2m}^{C2}}^{t_{2m+1}^{C2}} I_{out} \cdot \sin(\omega t) \cdot dt \quad (2)$$

Where I_{out} represents the amplitude of the output current, ΔQ_m^{C1} and ΔQ_m^{C2} are the discharge amount of the capacitors during mth cycle, and ω = 2 π f_{ref}. The total amount of electrical charge drawn from each capacitor (Q_{total}) can be expressed as:

$$Q_{total}^{C1} = \sum_0^n \Delta Q_m^{C1} = \sum_0^n \left(\int_{t_{2m}^{C1}}^{t_{2m+1}^{C1}} I_{out} \cdot \sin(\omega t) \cdot dt \right) \quad (3)$$

$$Q_{total}^{C2} = \sum_0^n \Delta Q_m^{C2} = \sum_0^n \left(\int_{t_{2m}^{C2}}^{t_{2m+1}^{C2}} I_{out} \cdot \sin(\omega t) \cdot dt \right) \quad (4)$$

Regardless of the increase in capacitors voltages at level ±2,

assuming the worst case in which no charge is absorbed by the capacitors, the minimum allowable capacitance can be formulated as:

$$C_{1\min} = \frac{Q^{C_1}}{V_{\text{ripple}}^{C_1}}, \quad C_{2\min} = \frac{Q^{C_2}}{V_{\text{ripple}}^{C_2}} \quad (5)$$

By assuming V_{ripple}^C below 10%, recovery of the capacitors voltage at levels 0 and ± 2 will be assured. Also, it is noticeable that no capacitors are charged or discharged at level ± 1 .

B. Power Loss Study

Power loss of the proposed converter can generally be classified into three categories:

- Switching losses (P_{sw})
- Conduction losses (P_{cond})
- Capacitor voltage ripple (charging) losses

In the following, a brief discussion of each category and its impact on efficiency in different load conditions is presented.

1) Switching loss

Switching energy losses of IGBTs (E_{sw}) in each switching cycle consist of turn-on loss (E_{on}) and turn-off loss (E_{off}). Switching losses are inherent characteristics of IGBTs, specified by the manufacturer under predefined conditions. These losses vary under different circumstances, including: junction temperature (T_j), collector current (I_c), blocking voltage (V_b), gate-emitter voltage (V_{GE}) and gate resistance (R_{GE}). Therefore, the E_{sw} can be calculated as:

$$E_{\text{sw}} = (E_{\text{on}} + E_{\text{off}}) \cdot \text{adj}_{T_j} \cdot \text{adj}_{I_c} \cdot \text{adj}_{V_b} \cdot \text{adj}_{V_{\text{GE}}} \quad (6)$$

In which E_{on} and E_{off} are losses presented by the IGBT module datasheet in nominal condition and adj_{T_j} , adj_{I_c} , adj_{V_b} and $\text{adj}_{V_{\text{GE}}}$ are adjustment factors for the aforementioned variable conditions. Therefore, the total switching power loss for the nine switches (P_{sw}) can be defined as:

$$P_{\text{sw}} = \sum_{k=1}^9 P_{\text{sw}_k} = \sum_{k=1}^9 E_{\text{sw}_k} \cdot f_{\text{ref}} \cdot N_k \quad (7)$$

N_k is the number of times each switch is turned on and off in one cycle of reference waveform. Switches S_1 , S_2 , S_3 and S_4 turn on and off once per each PWM cycle while $|A_{\text{ref}} \sin(\omega t)| \leq A$ and stay on or off for the rest of the reference cycle time. S_5 , S_6 , S_7 and S_8 turn on and off once per each 2 PWM cycles. While, S_9 turn on and off once for every PWM cycles. Thus:

$$N_k = \begin{cases} 2f_{\text{PWM}} \frac{\sin^{-1} \sin\left(\frac{A}{A_{\text{ref}}}\right)}{\pi f_{\text{ref}}} & k = 1, 2, 3, 4 \\ \frac{f_{\text{PWM}}}{2f_{\text{ref}}} & k = 5, 6, 7, 8 \\ \frac{f_{\text{PWM}}}{f_{\text{ref}}} & k = 9 \end{cases} \quad (8)$$

2) Conduction loss

Conduction losses occur due to current passing through circuit components. In the proposed structure, the conduction losses are the result of capacitors' internal resistance (R_{ESR}) losses and IGBTs/diodes losses. IGBT losses can be calculated by multiplying the IGBT collector-emitter voltage (V_{CE}) and collector current (I_c). Likewise, Diode losses are the result of

the forward voltage drop (V_F) while it conducts current (I_F). The output characteristics of IGBT (V_{CE}) and Diode (V_F) change at different current and operation conditions. V_{CE} and V_F can be calculated as follows:

$$V_{\text{CE}} = V_{\text{CE0}} + R_{\text{CE}} \cdot I_c \quad (9)$$

$$V_F = V_{F0} + R_D \cdot I_F \quad (10)$$

V_{CE0} and R_{CE} are the adjusted IGBT parameters represent the nonlinear relation between V_{CE} and I_c at circuit operation conditions. similarly, V_{F0} and R_D are adjusted Diode internal voltage drop and resistance, respectively. Therefore, equivalent circuits of the proposed topology and its conductive loss factors for each output levels are brought in Table II. It is worth mentioning that loss factors R_L and V_L represent the path resistance and internal voltage drop of semiconductor devices for each level of the output, respectively.

TABLE II
CIRCUIT CONDUCTIVE LOSS FACTORS

Vout Level	Equivalent Circuit	Loss factors	
		V_L	R_L
0 V _{dc}	1 IGBT & 1 Diode	$V_{\text{CE0}} + V_{F0}$	$R_{\text{CE}} + R_D$
± 1 V _{dc}	2 IGBTs & 2 Diodes	$2(V_{\text{CE0}} + V_{F0})$	$2(R_{\text{CE}} + R_D)$
± 2 V _{dc}	3 IGBTs, 1 Diode & 1 Capacitor	$3V_{\text{CE0}} + V_{F0}$	$3R_{\text{CE}} + R_D + R_{\text{ESR}}$
± 3 V _{dc}	4 IGBTs & 2 Capacitors	$4V_{\text{CE0}}$	$4R_{\text{CE}} + 2R_{\text{ESR}}$

According to Fig. 2, while $|A_{\text{ref}} \sin(\omega t)| \leq A$, the output goes back and forth between levels $L=0$ & 1. Similarly, the output alternate between levels $L=1$ & 2 and $L=2$ & 3 while $A \leq |A_{\text{ref}} \sin(\omega t)| \leq 2A$ and $2A \leq |A_{\text{ref}} \sin(\omega t)| \leq 3A$, respectively. For $L=0$, 1 and 2, the energy loss occurring in the aforementioned states can be defined as follows [21]:

$$E_{\text{cond}}^{L \& L+1} = \int_{t_i}^{t_j} \left[I_{\text{out}} \sin(\omega t) \right]^2 \left[\begin{aligned} & R_{L+1} \frac{A_{\text{ref}} \sin(\omega t) - L \times A}{A} + \\ & R_L \left(1 - \frac{A_{\text{ref}} \sin(\omega t) - L \times A}{A} \right) \\ & + \left[I_{\text{out}} \sin(\omega t) \right] \left[\begin{aligned} & V_{L+1} \frac{A_{\text{ref}} \sin(\omega t) - L \times A}{A} + \\ & V_L \left(1 - \frac{A_{\text{ref}} \sin(\omega t) - L \times A}{A} \right) \end{aligned} \right] \end{aligned} \right] dt \quad (11)$$

Energy loss happens at the following time intervals:

$$[t_i - t_j]: \begin{cases} [t_0 - t_1], [t_4 - t_5], [t_5 - t_6], [t_9 - t_{10}] & L = 0 \\ [t_1 - t_2], [t_3 - t_4], [t_6 - t_7], [t_8 - t_9] & L = 1 \\ [t_2 - t_3], [t_7 - t_8] & L = 2 \end{cases} \quad (12)$$

In which $t_1 = \frac{1}{\omega} \text{Arcsin}\left(\frac{A}{A_{\text{ref}}}\right)$, $t_2 = \frac{1}{\omega} \text{Arcsin}\left(\frac{2A}{A_{\text{ref}}}\right)$, $t_5 = \pi/\omega$, $t_{10} = 2\pi/\omega$, $t_3 = t_5 - t_2$, $t_4 = t_5 - t_1$, $t_6 = t_5 + t_1$, $t_7 = t_5 + t_2$, $t_8 = t_{10} - t_2$ and $t_9 = t_{10} - t_1$. Ultimately, the total conduction loss is:

$$P_{\text{cond}} = f_{\text{ref}} (4E_{\text{cond}}^{L \& 1} + 4E_{\text{cond}}^{L \& 2} + 2E_{\text{cond}}^{L \& 3}) \quad (13)$$

3) Capacitor voltage ripple losses

The power losses caused by the difference between the input and capacitors voltages, while they are paralleled to the source can be calculated as follows:

$$P_C = \frac{1}{2} \sum_{k=1}^u C_k \Delta V_k^2 f_{ref} \quad (14)$$

In which, u represents the number of both capacitors' charging states and then, ΔV_k is charging Voltage ripple of the capacitors. Finally, based on [21, 23], total power loss (P_{loss}) and efficiency (η) of the proposed converter can be calculated as follows:

$$P_{loss} = P_{sw} + P_{cond} + P_{C1} + P_{C2} \quad (15)$$

$$\eta = \frac{P_{out}}{P_{out} + P_{loss}} \times 100 \quad (16)$$

C. Comparison with other topologies

Table III reveals a detailed comparison over the proposed structure and other existing ones, in terms of number of circuit components (switches, driver circuits, capacitors, and diodes), number of input sources, Peak Inverse Voltage (PIV), Total Standing Voltage (TSV), regenerative load ability and the boosting ratio. PIV implies the maximum voltage which the switch has to bear in the off-state. In some applications, the number of switches may be low but some of the switches have to work with high voltages. Besides, TSV is the sum of standing/operating voltage (or simply sum of the PIV) of all the switches that should also be considered. Boost ratio is defined as the proportion of the output amplitude to the input source or the sum of input sources in case if there is more than one source is used.

In the context of step-up SC-MLI, it is essential to design a topology to use maximum possible standard rating of the switches. Therefore, reducing the number of switches by

increasing the standing voltage in standard range is an important aspect which should be considered in comparison. In fact, the input voltage could be raised until the PIV is less than a certain acceptable percentage ($x\%$) of the switches rated voltage (V_{rated}^{SW}) as follows:

$$PIV < x\% \cdot V_{rated}^{SW} \quad (17)$$

As can be seen in the Table III, unlike the proposed circuit, authors in [3], [31] and [32] introduced structures that require several isolated DC sources and the amplitude of the output does not exceed the sum of input voltages. In case of [3] and [32], it should be noted that using symmetric sources leads to a 5-level output waveform.

Although [20], [28] and [38-41] are single-source topologies with voltage boosting ability and have relatively less semiconductor devices (except for [28]), they cannot supply regenerative loads. [26] and [34-37] present single source structures with a considerably low TSV. However, they either cannot boost the input voltage, or they have a low boosting ratio. Also, they require more capacitors.

It is noticeable that topologies presented in [23], [24], and [33] can meet both the boost ratio and regenerative capability requirements, whereas the introduced SCMLI requires less active switches and, therefore, less gate driver circuits for the same output levels. Considering semiconductor count, boost factor, and regenerative load ability, the proposed topology should compete with [23], [24], and [33].

Selecting each switching device in an inverter is related to the maximum voltage impressed and the peak and average current going through it. Therefore, the product of voltage stress

TABLE III
COMPARISON OF THE SUGGESTED SEVEN-LEVEL INVERTER WITH RECENT TOPOLOGIES

NO.	Topology	N levels	N switches	N diodes	N drivers	N capacitors	N sources	PIV (*V _{in})	TSV (*V _{in})	Boost ratio	Regenerative	P _{out} (W)	Efficiency (%)	
													Theoretical	Experimental
1	[31] 2018	7	10	10	7	0	3	3	19	1x	Yes	50	N.A.	97.6
2	[32] 2017	7	8	8	8	0	2	2	12	1x	Yes	250 1000	N.A.	97 98
3	[3] 2017	7	8	8	8	0	2	3	18	1x	Yes	100	N.A.	94.3
4	[26] 2015	7	7	9	7	3	1	1	5	1x	Yes	500	N.A.	91
5	[34] 2017	7	12	12	12	4	1	1	3.33	1x	yes	500	N.A.	N.A.
6	[35] 2012	7	14	14	12	5	1	1	3.33	1x	yes	5000	N.A.	N.A.
7	[36] 2018	7	10	10	8	3	1	1	8	1.5x	yes	225	N.A.	N.A.
8	[37] 2019	7	10	10	8	4	1	1	7.5	1.5x	yes	266.2	96.5	96.5
9	[33] 2018	7	16	16	14	2	1	1	16	3x	Yes	40	N.A.	94
10	[23] 2014	7	10	10	10	2	1	3	18	3x	Yes	3.5	94.6	95.4
11	[24] 2016	7	16	16	14	2	1	1	16	3x	Yes	200 1000	93.8 90.2	N.A.
12	Proposed	7	9	12	9	2	1	3	17	3x	Yes	50 250 500	96.07 95.3 94.5	92 94.3 92.2
13	[38] 2018	7	9	10	8	3	1	1	7.5	1.5x	No	218	N.A.	97.29
14	[20] 2014	7	7	11	7	2	1	3	21	3x	No	247.5	N.A.	89.2
15	[28] 2018	7	14	14	14	2	1	1	14	3x	No	182.4	91.7	88.93
16	[39] 2019	7	8	6	8	2	1	3	18	3x	No	N.A.	N.A.	N.A.
17	[40] 2019	7	8	10	8	2	1	3	16	3x	No	189	N.A.	97.1
18	[41] 2014	7	8	10	8	2	1	3	18	3x	No	N.A.	N.A.	N.A.

and current stress is introduced as Switching Device Power (SDP) index [42]. The sum of SDP of all the switching devices used in the circuit is an important factor of an inverter. Considering the number of switching devices used (N), the peak voltage impressed on the devices (V_k), $I_{k,average}$ and $I_{k,peak}$ as the average and peak current through the device, respectively, then:

$$Total\ Average\ SDP = SDP_{avg} = \sum_{k=1}^N V_k \cdot I_{k,average} \quad (18)$$

$$Total\ Peak\ SDP = SDP_{peak} = \sum_{k=1}^N V_k \cdot I_{k,peak} \quad (19)$$

The SDP of all topologies with boosting ability for the same conditions including semiconductor device properties, output power ($P_{out}=750W$, $V_{out_max}=375V$), load power factor ($PF=1$) and input voltage ($V_{in}=125V$) are summarized as depicted in Fig. 3. As the number of semiconductors decreases, the amount of SDP_{ave} increases. Thus, non-regenerative structures with less semiconductors have a higher SDP_{ave} . Furthermore, for the Switched-Capacitor Structures the amount of SDP_{peak} directly depends on the resistance of capacitors charging paths. Changes in the charging paths resistance changes the peak current of the

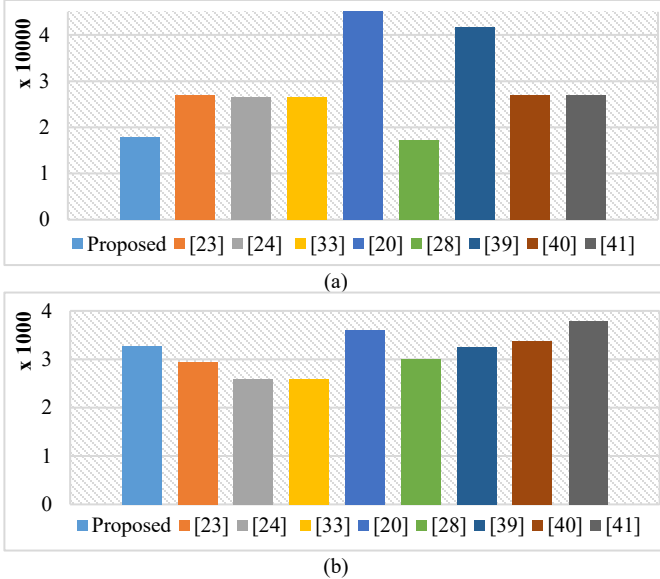


Fig. 4. Calculation results for (a) SDP peak and (b) SDP average

semiconductors. However, as (14) shows, it does not affect the capacitors charging loss. Consequently, the corresponding SDP_{peak} of the proposed SCMLI is better than the other topologies whereas its SDP_{ave} is within the range of them.

IV. EXPERIMENTAL RESULTS

In this section, the design characteristics and experimental results of the proposed 7-level inverter under various conventional (static and transient) and regenerative load conditions are discussed. In order to verify the feasibility of the proposed topology and assess its performance, a laboratory prototype is implemented (see Fig 4). Furthermore, the specifications of this setup are brought in Table IV. A TMS320F28335 DSP processor was used to create gate pulses based on the phase disposition technique. Then, these pulses were isolated and amplified by a circuit consisting of

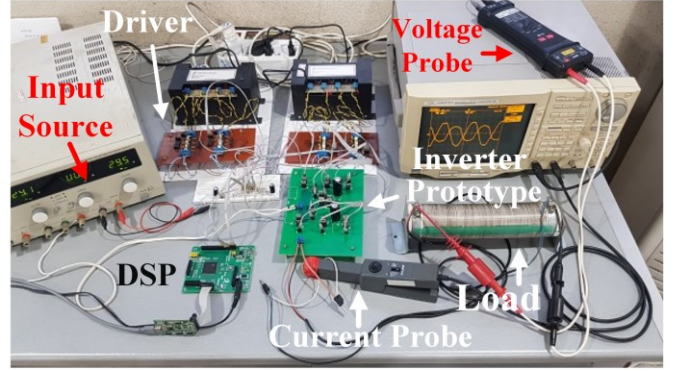


Fig. 3. Laboratory prototype of the proposed structure

TABLE IV
SPECIFICATIONS OF THE LAB PROTOTYPE PARAMETERS

Parameter/ Component	Value
Input Voltage	60V
Number of voltage levels	7
Maximum output voltage	180V
modulation index	0.9
Output Frequency	50Hz
PWM Frequency	3KHz
IGBT / Diode	12N60 / MUR860
Capacitors	C1=C2= 2200μF

HCPL3120 isolator IC.

When the phase difference between load voltage and current is below 90° ($0 \leq \phi < 90$), their polarity are the same for most of the cycle. Thus, the average power is supplied to the load and the overall performance of the inverter is considered to be inverting. Whenever the phase difference between load voltage and current is above 90° ($90 < \phi < 180$), their polarity differs for most of the cycle. Hence, the inverter pumps average power from the AC to the DC side and the overall performance of the inverter is considered to be rectification (or regeneration) [22]. This feature is crucial in switched-capacitor structures to prevent the capacitors from over-charge, feeding the excess charge to the input source, instead.

A. Inverting mode

Fig. 5.a depicts the output voltage and current waveforms of the proposed converter for a pure resistive load of $R=47.5\Omega$ and the output frequency of 50Hz. An input voltage of 60V was used to supply the converter, boosting it three times up to 180V. The modulation index is set to $M=0.9$. In the presence of a resistive-inductive load of $R=47.5\Omega$ and $L=103mH$, the output waveform is illustrated in Fig. 5.b. The input current waveform of the inverter (I_{in}) can be seen in Fig. 5.c. Note that the input current increases while the circuit capacitors are being charged. In this case, the experimental harmonic spectrum of the output voltage is shown in Fig. 6. It can be seen that the amplitude of all unwanted harmonics are kept below 5% satisfying the IEEE-Std. 519-2014 (except for the 60th harmonic, which is due to the switching frequency). Also, the THD for the first 50 harmonic orders is 7.056%. Moreover, voltage and current waveforms of the inverter capacitors are presented in Fig. 7 for five continuous cycles. It can be seen that having about a 4V ripple, the capacitors' voltages are well balanced. Additionally, for a

pure inductive load of $L=103\text{mH}$, Fig. 8.a shows the inverter's output voltage and current. To investigate the performance of the proposed topology under nonlinear load conditions, it was exposed to a single phase rectifier with RL load. Fig.8.b shows the output voltage and current waveforms of the inverter after being rectified over a resistive-inductive load ($R=47.5\Omega$ and $L=103\text{mH}$).

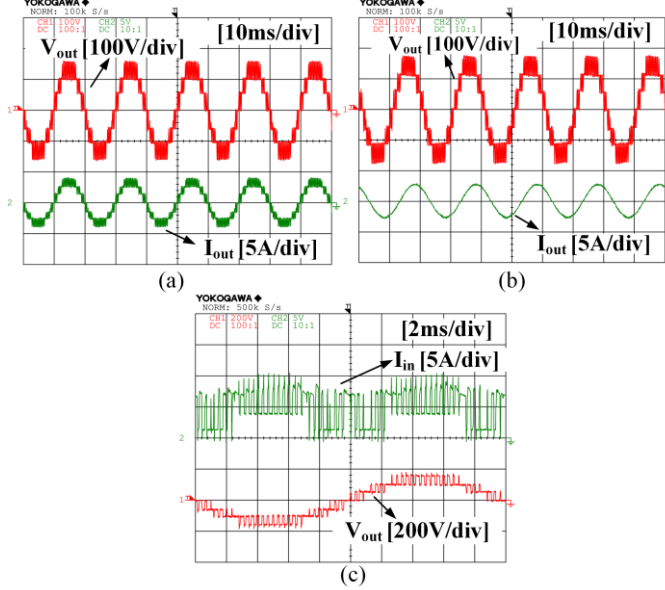


Fig. 5. Output voltage and current waveforms for (a) pure resistive load of $R=47.5\Omega$ (b) resistive-inductive load of $R=47.5\Omega$ and $L=103\text{mH}$ and (c) Input current of the inverter

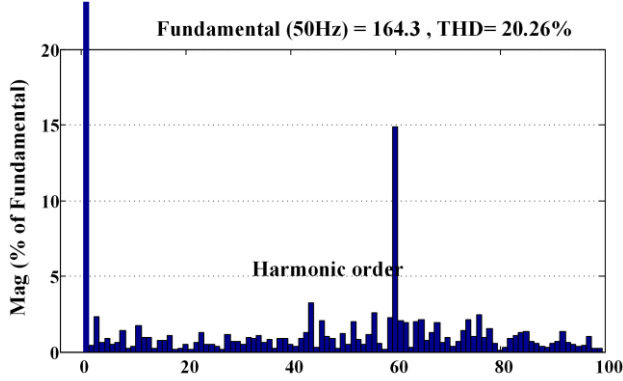


Fig. 6. experimental harmonic spectrum of the output voltage

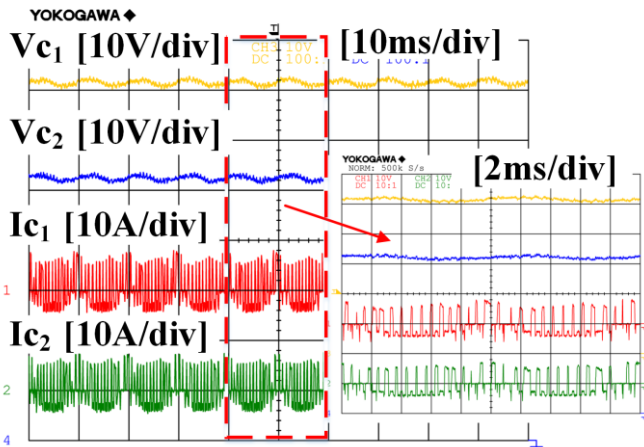


Fig. 7. Voltage and current waveforms of the inverter capacitors

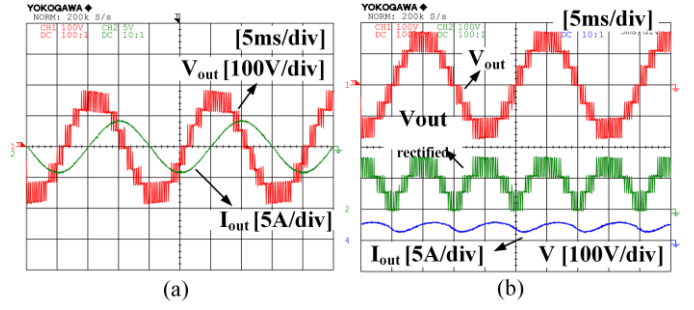


Fig. 8. Output voltage and current for (a) a pure inductive load ($L=103\text{mH}$) (b) Output waveforms of the inverter after being rectified

To test the proposed inverter in transient load conditions, different load transition cases have been studied. These tests suggest the proper performance of the inverter. Fig. 9.a and b show the effects of sudden load change from Resistive ($R_1=95\Omega$) to ($R_2=R_1||95\Omega$). The frequency of this periodic load transition is 1Hz. Fig. 10 shows the collector-emitter voltage of two selected inverter switches (V_{S1} and V_{S5}). H-bridge switches (V_{S1}) have to withstand the output voltage but the rest of the switches only should bear the input voltage at most.

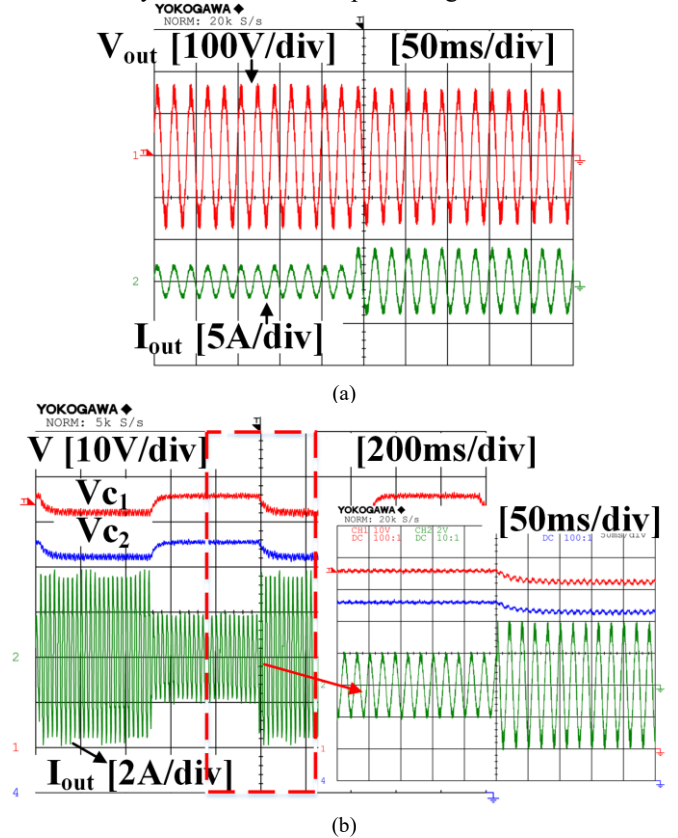


Fig. 9. Load waveforms under sudden change (a) output voltage and current (b) capacitors voltages and the load current

B. Regenerative performance

In order to demonstrate the regenerative load performance of the proposed inverter, a test setup is devised as depicted in Fig. 11. The proposed inverter is connected to an H-bridge inverter via a line impedance (z) with the value of ($R=2\Omega$, $L=107\text{mH}$).

Fig. 12 illustrates the experimental results under regenerative load condition. Fig. 12.a presents the V_{load} and I_{load} , where they

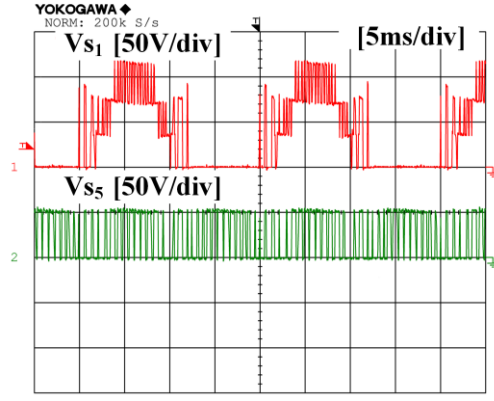


Fig. 10. Collector-emitter voltage across the switches S_1 and S_5

have a phase difference of more than 120° (lag). It also shows V_H which has the same RMS value as V_{load} with 15° leading phase difference. Voltage ripple and current waveform of the capacitor C_1 is depicted in Fig. 12.b under such conditions. Note that, the capacitor C_1 is being charged from the output and is feeding the excess power back to the DC source as depicted in Fig. 12.c, where I_{in} is negative for the most part. It goes exactly the same for the capacitor C_2 .

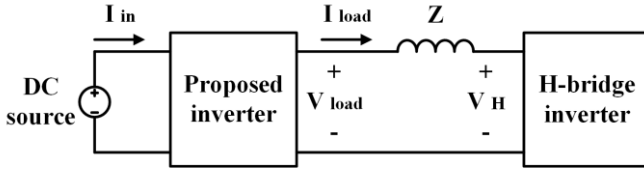


Fig. 11. Circuit diagram for regenerative performance test

The experimental and theoretical efficiency of the proposed converter for different output powers is plotted in Fig. 13, which they reach 94.3 and 96.07 percent at peak, respectively. It can be seen the efficiency of the converter is above 92% over a wide range of output power.

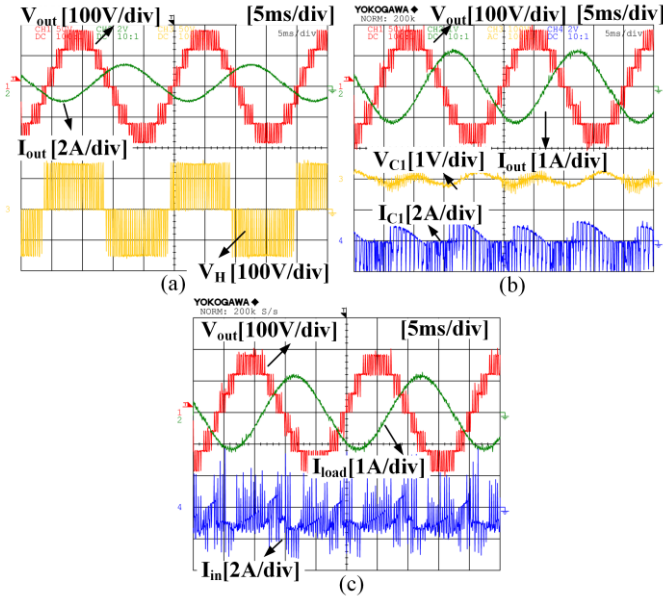


Fig. 12. Experimental results under regenerative load condition (a) V_{load} , I_{load} and V_H (b) V_{C1} and I_{C1} and (c) I_{in}

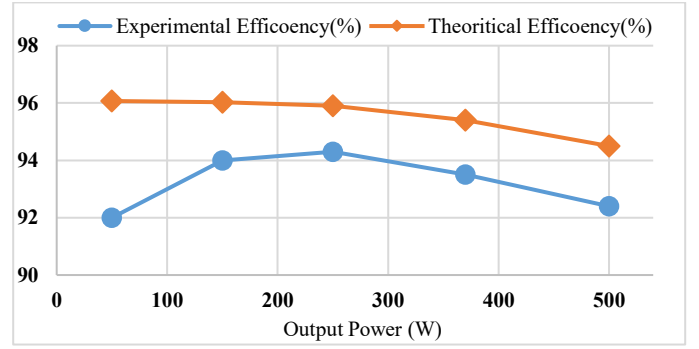


Fig. 13. Experimental and theoretical efficiency of the proposed converter for different output powers

V. CONCLUSION

A new step-up single-source seven-level inverter topology aiming for circuit component reduction, including power and control circuit was introduced in this report. The proposed structure boosts the supply voltage based on switched-capacitor concept by charging capacitors and combining them to generate the intended output. Applying the PD-PWM method led to not only an output with better quality but also lower stresses on circuit components. Self-voltage balancing and high efficiency were achieved by implementing the proposed concept under different operating conditions. Experimental results prove that the structure performs appropriately under regenerative load condition by feeding the excess charge of the capacitors back to the input source. Moreover, a comparison to other recent topologies revealed that lower semiconductor counts and a simpler circuit were realized, considering the regenerative load feature, boost ratio, and TSV. Regarding the abovementioned pros, this circuit mostly suits for low voltage renewable application.

REFERENCES

- [1] N. Sandeep and U. R. Yarangatti, "A switched-capacitor-based multilevel inverter topology with reduced components," *IEEE Trans. Power Electron.*, 2017.
- [2] A. Emadi, S. S. Williamson, and A. Khaligh, "Power electronics intensive solutions for advanced electric, hybrid electric, and fuel cell vehicular power systems," *IEEE Trans. Power Electron.*, vol. 21, no. 3, pp. 567–577, 2006.
- [3] R. Uthirasamy, V. K. Chinnaiyan, U. S. Ragupathy, and J. Karpagam, "Investigation on three-phase seven-level cascaded DC-link converter using carrier level shifted modulation schemes for solar PV system applications," *IET Renew. Power Gener.*, vol. 12, no. 4, pp. 439–449, 2017.
- [4] L. M. Tolbert and F. Z. Peng, "Multilevel converters for large electric drives," in *Applied Power Electronics Conference and Exposition, 1998. APEC'98. Conference Proceedings 1998.*, Thirteenth Annual, 1998, vol. 2, pp. 530–536.
- [5] Y. Hinago and H. Koizumi, "A switched-capacitor inverter using series/parallel conversion with inductive load," *IEEE Trans. Ind. Electron.*, vol. 59, no. 2, pp. 878–887, 2012.
- [6] F. Shahnazian, J. Adabi, E. Pouresmaeil, & J. P. "Catalão. Interfacing modular multilevel converters for grid integration of renewable energy sources", *Electric Power Systems Research*, 160, 439-449, 2018.
- [7] K. V. Iyer, R. Baranwal, and N. Mohan, "A high-frequency AC-link single-stage asymmetrical multilevel converter for grid integration of renewable energy systems," *IEEE Trans. Power Electron.*, vol. 32, no. 7, pp. 5087–5108, 2017.
- [8] A. Mokhberdoran and A. Ajami, "Symmetric and asymmetric design and implementation of new cascaded multilevel inverter topology," *IEEE Trans. power Electron.*, vol. 29, no. 12, pp. 6712–6724, 2014.

- [9] A. Nabae, I. Takahashi, and H. Akagi, "A new neutral-point-clamped PWM inverter," *IEEE Trans. Ind. Appl.*, no. 5, pp. 518–523, 1981.
- [10] T. A. Meynard and H. Foch, "Multi-level choppers for high voltage applications," *EPE J.*, vol. 2, no. 1, pp. 45–50, 1992.
- [11] E. Babaei and S. S. Gowgani, "Hybrid multilevel inverter using switched capacitor units," *IEEE Trans. Ind. Electron.*, vol. 61, no. 9, pp. 4614–4621, 2014.
- [12] M. Malinowski, K. Gopakumar, J. Rodriguez, and M. A. Perez, "A survey on cascaded multilevel inverters," *IEEE Trans. Ind. Electron.*, vol. 57, no. 7, pp. 2197–2206, 2010.
- [13] K. K. Gupta and S. Jain, "Topology for multilevel inverters to attain maximum number of levels from given DC sources," *IET Power Electron.*, vol. 5, no. 4, pp. 435–446, 2012.
- [14] K.-M. Tsang and W.-L. Chan, "Single DC source three-phase multilevel inverter using reduced number of switches," *IET power Electron.*, vol. 7, no. 4, pp. 775–783, 2014.
- [15] P. Flores, J. Dixon, M. Ortúzar, R. Carmi, P. Barriuso, and L. Morán, "Static var compensator and active power filter with power injection capability, using 27-level inverters and photovoltaic cells," *IEEE Trans. Ind. Electron.*, vol. 56, no. 1, pp. 130–138, 2009.
- [16] G.-J. Su, "Multilevel DC-link inverter," *IEEE Trans. Ind. Appl.*, vol. 41, no. 3, pp. 848–854, 2005.
- [17] J. Rodriguez, S. Bernet, P. K. Steimer, and I. E. Lizama, "A survey on neutral-point-clamped inverters," *IEEE Trans. Ind. Electron.*, vol. 57, no. 7, pp. 2219–2230, 2010.
- [18] A. Khodaparast, J. Adabi, & M. Rezanejad, "A step-up switched-capacitor multilevel inverter based on 5-level T-type modules", *IET Power Electronics*, 12(3), 483–491, 2018.
- [19] K. K. Gupta, A. Ranjan, P. Bhatnagar, L. K. Sahu, and S. Jain, "Multilevel inverter topologies with reduced device count: a review," *IEEE Trans. Power Electron.*, vol. 31, no. 1, pp. 135–151, 2016.
- [20] Y. Ye, K. W. E. Cheng, J. Liu, and K. Ding, "A step-up switched-capacitor multilevel inverter with self-voltage balancing," *IEEE Trans. Ind. Electron.*, vol. 61, no. 12, pp. 6672–6680, 2014.
- [21] A. Khodaparast, E. Azimi, A. Azimi, M. E. Firouzjaee, J. Adabi, and E. Pouresmaeil, "A New Modular Multilevel Inverter Based on Step-Up Switched-Capacitor Modules," *Energies*, 12(3):524, 2019.
- [22] K. Bimal, "Bose," *Modern Power Electronics and AC drives*, Vol. 123. Upper Saddle River, NJ: Prentice hall, 2002.
- [23] A. Tsunoda, Y. Hinago, and H. Koizumi, "Level-and phase-shifted PWM for seven-level switched-capacitor inverter using series/parallel conversion," *IEEE Trans. Ind. Electron.*, vol. 61, no. 8, pp. 4011–4021, 2014.
- [24] X. Sun, B. Wang, Y. Zhou, W. Wang, H. Du, and Z. Lu, "A Single DC Source Cascaded Seven-Level Inverter Integrating Switched-Capacitor Techniques," *IEEE Trans. Ind. Electron.*, vol. 63, no. 11, pp. 7184–7194, 2016.
- [25] M. Saeedian, S. M. Hosseini, and J. Adabi, "A Five-Level Step-up Module for Multilevel Inverters: Topology, Modulation Strategy and Implementation," *IEEE J. Emerg. Sel. Top. Power Electron.*, 2018.
- [26] J.-S. Choi and F. Kang, "Seven-level PWM inverter employing series-connected capacitors paralleled to a single DC voltage source," *IEEE Trans. Ind. Electron.*, vol. 62, no. 6, pp. 3448–3459, 2015.
- [27] M. Saeedian, M. E. A. Firouzjaee, S. M. Hosseini, J. Adabi, and E. Pouresmaeil, "A novel step-up single source multilevel inverter: Topology, operating principle and modulation," *IEEE Trans. Power Electron.*, 2018.
- [28] A. Taghvaie, J. Adabi, and M. Rezanejad, "A self-balanced step-up multilevel inverter based on switched-capacitor structure," *IEEE Trans. Power Electron.*, vol. 33, no. 1, pp. 199–209, 2018.
- [29] R. Barzegarkhoo, H. M. Kojabadi, E. Zamir, N. Vosoughi, and L. Chang, "Generalized structure for a single phase switched-capacitor multilevel inverter using a new multiple DC link producer with reduced number of switches," *IEEE Trans. Power Electron.*, vol. 31, no. 8, pp. 5604–5617, 2016.
- [30] R. Wang, L. Shi, L. Yao, and Y. Ni, "Small signal stability analysis with high penetration of grid-connected wind farm of PMSG type considering the wake effect," in *PES General Meeting Conference & Exposition*, 2014 IEEE, 2014, no. 2, pp. 1–5.
- [31] S. S. Lee, M. Sidorov, N. R. N. Idris, and Y. E. Heng, "A Symmetrical Cascaded Compact-Module Multilevel Inverter (CCM-MLI) With Pulsewidth Modulation," *IEEE Trans. Ind. Electron.*, vol. 65, no. 6, pp. 4631–4639, 2018.
- [32] L. Ren, G. Chunying, H. Kaiyi, and Z. Yao, "Modified hybrid modulation scheme with even switch thermal distribution for H-bridge hybrid cascaded inverters." *IET Power Electronics* 10, no. 2: 261–268, 2017.
- [33] S. S. Lee, "A single-phase single-source 7-level inverter with triple voltage boosting gain." *IEEE Access* 6: 30005–30011, 2018.
- [34] Tian, Hao, Yuzhuo Li, and Yun Wei Li. "A novel seven-level hybrid-clamped (HC) topology for medium-voltage motor drives." *IEEE Transactions on Power Electronics* 33, no. 7: 5543–5547, 2017.
- [35] Saeedifard, Maryam, Peter Mantovanelli Barbosa, and Peter K. Steimer. "Operation and control of a hybrid seven-level converter." *IEEE transactions on power electronics* 27, no. 2: 652–660, 2011.
- [36] Liu, Junfeng, Xiangkai Zhu, and Jun Zeng. "A seven-level inverter with self-balancing and low voltage stress." *IEEE Journal of Emerging and Selected Topics in Power Electronics*, 2018.
- [37] Lee, Sze Sing, Yeongsu Bak, Seok-Min Kim, Anto Joseph, and Kyo-Beum Lee. "New Family of Boost Switched-Capacitor Seven-Level Inverters (BSC7LI)." *IEEE Transactions on Power Electronics* 34, no. 11: 10471–10479, 2019.
- [38] Liu, Junfeng, Jialei Wu, and Jun Zeng. "Symmetric/asymmetric hybrid multilevel inverters integrating switched-capacitor techniques." *IEEE Journal of Emerging and Selected Topics in Power Electronics* 6, no. 3: 1616–1626, 2018.
- [39] Roy, Tapas, and Pradip Kumar Sadhu. "A Step-up Multilevel Inverter Topology using Novel Switched Capacitor Converters with Reduced Components." *IEEE Transactions on Industrial Electronics*, 2020.
- [40] Peng, Wei, Qiang Ni, Xiaohuan Qiu, and Yuanmao Ye. "Seven-level inverter with self-balanced switched-capacitor and its cascaded extension." *IEEE Transactions on Power Electronics* 34, no. 12: 11889–11896, 2019.
- [41] Babaei, Ebrahim, and Saeed Sheermohammadzadeh Gowgani. "Hybrid multilevel inverter using switched capacitor units." *IEEE Transactions on industrial electronics* 61, no. 9: 4614–4621, 2013.
- [42] M. Shen, A. Joseph, J. Wang, F. Z. Peng and D. J. Adams, "Comparison of Traditional Inverters and Z -Source Inverter for Fuel Cell Vehicles," in *IEEE Transactions on Power Electronics*, vol. 22, no. 4, pp. 1453–1463, July 2007.



Aryorad Khodaparast was born in Ghaemshahr, Iran in 1991. He received the B.Sc., M.Sc. degrees in power engineering from Babol Noshirvani University of Technology, Babol, Iran, in 2013 and 2017, respectively. Currently, he is a researcher and teacher assistant at Babol Noshirvani University of Technology. His research interests include Switched-Capacitors circuits, power converters and their applications in renewable energy.



Javad Hassani was born in Babol, Iran in 1991. He received the B.Sc., M.Sc. degrees in power engineering from Babol Noshirvani University of Technology, Babol, Iran, in 2013 and 2017, respectively. Currently, he is a researcher at Noshirvani University of Technology, Babol, Iran. His current research interests are power electronics converters and Drive systems.



Erfan Azimi was born in Babol, Iran in 1991. He received the B.Sc. and M.Sc. power engineering in 2013 and 2016. Currently, he is a researcher at Noshirvani University of Technology, Babol, Iran. His current research interests are Power Converters, Micro-Grids, and Renewable Energy.



M. Ebrahim Adabi was born in 1985. He received the B.Sc. and M.Sc. degrees in Electrical Engineering in 2008 and 2011, and the Ph.D. degree in Electrical Engineering from Universitat Politècnica de Catalunya (UPC), Barcelona, Spain in 2018. He is currently a Postdoctoral Researcher with Ecole Centrale de Nantes in Laboratoire des

Sciences du Numériques de Nantes, Nantes, France. His research interests include design and modeling of power electronic converters for renewable energy applications, and modular multilevel converters.



Jafar Adabi was born in 1981. He received his BEng and MEng degrees from Mazandaran University, Babol, Iran, in 2004 and 2006, respectively. He finished his PhD degree in the School of Engineering Systems at the Queensland University of Technology, Brisbane, Queensland, Australia at 2010.

Currently, he is an associate professor at Babol Noshirvani University of Technology, Babol, Iran. His research interests are the optimal design and high frequency modelling of power electronics and motor drive systems for EMI analysis.



Edris Pouresmaeil (M'14-SM'17) received the Ph.D. degree in Electrical Engineering from Technical University of Catalonia (UPC-Barcelona Tech), Barcelona, Spain, in 2012. After his Ph.D., he joined the University of Waterloo, Waterloo, Canada as a Post-Doctoral Research Fellow and then

joined the University of Southern Denmark (SDU), Odense, Denmark, as an Associate Professor. He is currently an Associate Professor with the Department of Electrical Engineering and Automation (EEA) at Aalto University, Espoo, Finland. His main research activities focus on the application of power electronics in power and energy sectors.